Dynamic correlation functions for finite and infinite smectic-*A* systems: Theory and experiment

A. Poniewierski and R. Hołyst
Institute of Physical Chemistry and College of Science, Polish Academy of Sciences, Kasprzaka 44/52, 01-224 Warsaw, Poland

A. C. Price and L. B. Sorensen
Department of Physics, University of Washington, Seattle, Washington 98195

S. D. Kevan and J. Toner
Department of Physics, University of Oregon, Eugene, Oregon 97403

(Received 24 December 1997)

In this paper, we present the dynamic layer displacement–layer displacement and the dynamic density-density correlation functions—both for smectic-*A* systems in the thermodynamic limit, and for real smectic-*A* films that have finite size, nonzero surface tension acting at the two free surfaces, and nonzero layer sliding viscosity. We also present the results of our soft-x-ray photon correlation spectroscopy experiment, which we have used to directly measure the dynamic density-density correlation function for two different liquid crystals (4O.8 and 7O.7) in the overdamped surface tension restoring force limit of our theory. We used linearized hydrodynamics to first calculate the behavior of smectic-*A* systems in the thermodynamic limit, and then to calculate the behavior for real, finite size, nonzero surface tension freely suspended liquid crystal films. For the real films, we used the linearized smectic-*A* hydrodynamic equations and the Gaussian model for the layer fluctuations to compute the set of relaxation times for the displacement field in a finite smectic-*A* film bounded by two free surfaces. We find that all of the relaxation times have maxima at nonzero values of the transverse wave vector $\mathbf{q}_\perp$. For thicker films the maxima shift towards $\mathbf{q}_\perp = \mathbf{0}$ and grow linearly with the number of smectic layers $N+1$. For finite N all of the relaxation times tend to zero as $q_\perp \to 0$, except one that attains the finite value $\tau^{(0)}(0) = (N+1)\eta_3 d/2\gamma$, where η_3 is the layer sliding viscosity, d is the smectic period, and γ is the surface tension. We find that the time-dependent scattering intensity integrated over $\mathbf{q}_\perp$ has the simple scaling form $S(q_z,t) \sim (a_0/\Lambda)^{y(t)}$, where a_0 and Λ are the molecular size cutoff and the instrument resolution cutoff, respectively, and the time-dependent exponent $y(t) = (k_B T q_z^2/4\pi\gamma)[1-\exp(-t/\tau^{(0)}(0))]$. Our results clearly show that the boundary conditions strongly affect the hydrodynamics of real smectics.
[S1063-651X(98)10408-7]

PACS number(s): 61.30.Cz, 83.70.Jr

I. INTRODUCTION

The six three-dimensional fluid smectic liquid crystals—namely, the two untilted smectic-*A* and hexatic-*B* phases, and the four tilted smectic-*C*, smectic-*F*, smectic-*I*, and smectic-*L* phases—are the only systems that we have which are precisely at their lower marginal dimensionality in three dimensions, i.e., for these systems $d^0 = 3$. Consequently, there has been some beautiful, seminal theoretical [1] and experimental [2] work on the nonuniversal algebraic decay of the static density-density correlation functions in the smectic-*A* phase. This algebraic decay of the static correlation functions is produced by the divergent thermal fluctuations that occur in a system that is precisely at its lower marginal dimensionality. These six smectic phases at their lower marginal dimensionality can each be thought of as an extended line of critical points. On the other hand, what are the dynamic correlation functions, and how can we measure them, in a system that is precisely at its lower marginal dimensionality?

There has also been some recent work [3–5] bridging the gap between the algebraic singularities in the static correlation functions—which only occur in the thermodynamic limit—and the actual nondivergent behavior that occurs in real, finite-size, nonzero surface tension, nonzero viscosity systems. Surprisingly, the effects of the Landau-Peierls fluctuations, which destroy the long-range order in the thermodynamic limit, also produce substantial effects in extremely thin liquid crystal films [3–5], but the crossover to the thermodynamic limit is extremely slow. This extraordinary large-length-scale crossover also occurs in two-dimensional melting. For example, it was originally suggested [6] that the required system size to observe Kosterlitz-Thouless-Halperin-Nelson-Young melting in helium was about $10^{13} \times 10^{13}$ lattice constants, or about 500 m by 500 m, and that the associated time scales would be extremely slow. Shortly afterwards, it was shown [7] that the required system size was ''only'' about $10^8 \times 10^8$ lattice constants, or about 0.5 mm by 0.5 mm. Of course, all of the definitive experiments were done with effective system sizes less than about $10^3 \times 10^3$ lattice constants, or about 2000 Å by 2000 Å. One of the most important lessons of this era was that finite-size systems could be used to measure, and to calculate, the precursor behavior long before the thermodynamic limit.

Although the bulk smectic-*A* phase is always technically at lower marginal dimensionality, the layer compression elastic constant B grows rapidly away from the nematic-to-smectic-*A* transition [8], and consequently over much of the phase we must go to extremely large system sizes before the root-mean-square layer fluctuation amplitude $\langle u^2 \rangle^{1/2}$ be-

comes comparable to the layer spacing d. The three-dimensional liquid crystal version [3,5] (i.e., the theory for a finite-size smectic-A system embedded in three-dimensional space) of the two-dimensional melting calculation predicts that

$$\langle u^2\rangle^{1/2}=\left[\frac{k_BT}{4\pi\sqrt{KB}}\ln(L/a_0)\right]^{1/2}\approx(2.5\ \text{Å})\sqrt{\ln(L/a_0)}, \tag{1}$$

where K is the layer bend elastic constant, L is the linear size of the sample, and a_0 is a molecular size beyond which the elastic theory breaks down. The above 2.5 Å is obtained for $k_BT=4\times10^{-14}$ erg and for typical smectic-A parameters: $B=2.5\times10^7$ dyn/cm^2 and $K=10^{-6}$ dyn. We also assume that the molecular cutoff $a_0=5$ Å and the layer spacing $d=30$ Å. This equation predicts that the size of the system must be about the same as the size of the earth before the rms layer fluctuation amplitude is equal to about one-half of the layer spacing, and that it must be about 2×10^{52} m, which is about 2×10^{37} light years—or about 2×10^{27} times larger than the estimated current diameter of the universe, which is about 10^9 light years—before the rms layer fluctuation amplitude is equal to the layer spacing. The main point here, of course, is that the logarithmic divergence is extremely slow. It is clearly impossible to do experiments on systems this large—or to turn off the surface tension, or to turn off the viscosity. Consequently, it is important to understand what happens in real, finite-size samples with both surface tension and viscosity included.

Although there has been beautiful theoretical and experimental work on the static correlation functions, there has been very little work on the dynamic correlation functions. Our goal in this paper is to answer three of the obvious fundamental questions about the dynamic critical behavior of the smectic-A phase, namely (i) What is the dynamic layer displacement–layer displacement correlation function, and what is the corresponding density-density correlation function, for the smectic-A phase in the thermodynamic limit? (ii) What happens in real samples, i.e., what are the effects of finite-system size, nonzero surface tension, and nonzero viscosity on the dynamic displacement-displacement and the dynamic density-density correlation functions? (iii) How can we probe the dynamic density-density correlation function in the smectic-A phase experimentally? We will answer these three questions, one at a time, in the next three sections. Surprisingly, we find that the effects of finite-system size and of nonzero surface tension on the dynamics of the Landau-Peierls fluctuations are much larger than their effects on the statics. On the experimental side, this is still a work in progress. We have measured the thermally driven fluctuations for two different liquid crystals in the overdamped limit, where the restoring force is due to the surface tension γ, and the damping is due to the layer sliding viscosity η_3. However, our results indicate that we will also be able to use our technique—which is soft-x-ray photon correlation spectroscopy—to measure the thermally driven fluctuations where the layer compression elastic constant B and the layer bend elastic constant K provide the restoring forces, and the layer sliding viscosity η_3 provides the damping.

The four hydrodynamical variables in smectic-A liquid crystals are the density ρ, the velocity field $\mathbf{v}$, and the layer displacement field u, which is associated with the broken translational symmetry. One goal of this paper is to provide a detailed analysis of the dynamic displacement-displacement correlation function, including its relaxation time, both in the thermodynamic limit for bulk smectic-A systems, and in finite-size smectic-A films with surface tension.

Freely suspended smectic liquid crystal films are nearly perfect model systems for the study of the influence of the boundary conditions on the different static properties of the smectic phases. For example, the smectic layer fluctuations have been studied both by x-ray scattering [4,9,10] and by laser light scattering [11,12]. There have also been studies of the meniscus and the dislocations [13], and studies of the surface-induced phase transitions [14–16]. These studies have shown that both the nonzero surface tension and the finite size strongly influence the behavior of these systems. For example, when the surface tension is large, it quenches the smectic layer fluctuations, and this quenching produces an enhanced x-ray specular reflectivity—this clearly demonstrates that the static displacement-displacement correlation functions are strongly influenced by the surface tensions acting at the two free surfaces [3,4,5,10]. In this paper, we will discuss the influence of finite system size, surface tension, and viscosity on the dynamic correlation functions of smectic-A films.

The full hydrodynamic behavior of the smectic systems that we are interested in is very complicated since there are five viscosities involved [17]. Four of these diverge as ω^{-1} in the low-frequency limit [18]. These divergences are the direct consequence of the anharmonic terms in the elastic energy of the smectic-A phase, which are required by the rotational invariance of the free energy [19]. However, fortunately, there are a few limits where the hydrodynamics are reasonably simple. One simple regime occurs for very low-frequency ($\omega\leqslant50$ kHz) and long-wavelength ($\lambda\geqslant0.1$ cm) vibrations of freely suspended smectic-A films. Experimental studies [20,21] of the eigenfrequencies of vibrating films in this regime show that the equation of motion is just the simple wave equation

$$2\gamma\left(\frac{\partial^2u}{\partial x^2}+\frac{\partial^2u}{\partial y^2}\right)-\rho_0Nd\,\frac{\partial^2u}{\partial t^2}=0. \tag{2}$$

Here, u is the vertical displacement of the film from its equilibrium position, ρ_0 is the density of the N-layer film, and the surface tension γ acts at the two free surfaces.

In their derivations of this simple wave equation, these authors [20,21] assumed that only the density changes—i.e., they assumed that both the permeation and the heat transfer can be neglected, and they also assumed that the internal structure of the film remained unchanged. The neglect of the changes in the internal structure is justified for long-wavelength, low-frequency vibrations because the curvature energy associated with K, and the layer compression energy associated with B, are both very small compared to the energy associated with the surface tension term. Using the typical values $d=30$ Å, $K=10^{-6}$ dyn, and $\lambda=0.1$ cm, we find

$$Kdq^2/\gamma\sim10^{-14}, \tag{3}$$

where $q=2\pi/\lambda$ is the modulus of the wave vector. The compression of the film can be neglected, because the elastic constant associated with compression is so large (typically $B\approx 10^7$ dyn/cm^2) that $B/d \gg 2\gamma q^2$. This means that the layers vibrate without appreciably changing their thicknesses [22]. Finally, we can also neglect the viscosity term in the equation of motion, for reasons that will be discussed in the next two sections.

However, when the wavelength of the vibrations gets smaller, and/or the thickness of the film gets larger, then the internal structure *will* play a non-negligible role. We can estimate [22] that this will start to happen when

$$\frac{2\gamma q_\perp^2 dN}{B} \sim 0.1. \tag{4}$$

Using our set of typical parameters above, we find that this crossover starts when

$$2.7\times 10^3 \sqrt{N} \approx \lambda_c \quad \text{(measured in Å)}. \tag{5}$$

For $N=100$, the typical crossover length is $\lambda_c = 2.7\ \mu$m. In the next section, we will concentrate on wavelengths that are smaller than this.

Another simple limit of the complicated hydrodynamics of the smectic-*A* phase is obtained when $\omega \sim q_z \sim q_\perp^2$. Here, q_z is the wave vector associated with compression of the layers, and $q_\perp$ is the wave vector associated with undulations of the layers. In this regime, the nonlinearities can be neglected and the hydrodynamics can be linearized [18]. This regime will be described in detail in the next section.

The remainder of this paper is organized as follows. In the second section, we will first discuss the simple linearized hydrodynamics of the bulk smectic-*A* phase, and then we will present the dynamic displacement–displacement and the dynamic density-density correlation functions for the smectic-*A* phase in the thermodynamic limit. In the third section, we will first present the equations that govern the layer fluctuations in finite smectic-*A* samples (again in the linearized regime), then we will discuss the relaxation times of the symmetric and the antisymmetric modes both for periodic boundary conditions and for free surface boundary conditions, and finally, we will present the dynamic displacement-displacement and the dynamic density-density correlation functions. In the fourth section, we will briefly present our experimental results for the overdamped surface tension modes, and we will show that our results agree with our theoretical predictions made in Sec. III. In the fifth section, we will present a discussion of our results and some of the possible future directions. The detailed mathematics behind the second and third sections is relegated to Appendix A and Appendix B, respectively.

II. THE DYNAMIC CORRELATION FUNCTIONS FOR THE SMECTIC-*A* PHASE IN THE THERMODYNAMIC LIMIT

The space- and time-dependent electron density $\rho_e(\mathbf{r},t)$ in the smectic-*A* phase is given—in the zeroth-order approximation, which neglects all of the higher-order Fourier components—by

$$\rho_e(\mathbf{r},t) = \text{const} + |\Psi(\mathbf{r},t)| \exp\{iq_0[z+u(\mathbf{r},t)]\} + \text{c.c.} \tag{6}$$

Here, $\Psi(\mathbf{r},t)$ represents the local amplitude of the density wave, $u(\mathbf{r},t)$ represents the local displacement field of the layers, $q_0=2\pi/d$ represents the wave number associated with the layer spacing d, the layers are perpendicular to the z axis, and c.c. denotes the complex conjugate of the second term. We note in passing that an electron density almost indistinguishable from the simple form given by Eq. (6) is obtained if we convolve the molecular center-of-mass probability distribution with the electron density of a single liquid-crystal molecule. The molecular center-of-mass distribution can be well approximated by the sum of Gaussian distributions, in which the ith Gaussian distribution is centered at the equilibrium position of the ith smectic layer z_i, and depends only on the distance from that layer $|z-z_i|$ [4]. Away from the nematic-to-smectic-*A* phase transition, we can neglect the fluctuations in the amplitude and concentrate on the layer displacement fluctuations. If we consider the Gaussian model of layer displacement fluctuations at time $t=0$, and linearized hydrodynamics, then the fluctuations of the local displacement field $u(\mathbf{r},t)$ will be Gaussian at all times. Consequently, the dynamic electron density-density correlation function, which is studied in our x-ray-scattering measurements, can be expressed as follows:

$$G_e(\mathbf{r},t) = |\Psi|^2 \exp\{-\tfrac{1}{2}q_0^2\langle[u(\mathbf{r},t)-u(\mathbf{r},0)]^2\rangle\}. \tag{7}$$

Here, $\langle\cdots\rangle$ denotes the thermal average using the appropriate Boltzmann factor associated with the full elastic energy. Note that it follows from this equation that in order to find the dynamic density-density correlation function, it is sufficient to compute the dynamic displacement-displacement correlation function.

The standard smectic-*A* elastic Hamiltonian is given by

$$H = \tfrac{1}{2}\int d^3r \left\{ B\left[\frac{\partial u(\mathbf{r})}{\partial z}\right]^2 + K[\Delta_\perp u(\mathbf{r})]^2 \right\}. \tag{8}$$

At $t=0$, we find that the standard static displacement-displacement correlation function, in the Fourier representation, is given by [1]

$$\langle u(\mathbf{q},0)u(-\mathbf{q},0)\rangle = \frac{k_BT}{Bq_z^2+Kq_\perp^4}. \tag{9}$$

Note that this equation implicitly tells us that the important wave-vector regime occurs when $q_z \approx q_\perp^2\sqrt{K/B}$. For typical thermotropic smectic-*A* materials, we find $\sqrt{K/B}\approx d$, and consequently, $q_z \ll q_\perp$. However, for the fluorinated thermotropic liquid crystals, B is much larger [10]. This means that, in both cases, the wavelengths of the thermally excited compression modes are much longer than the wavelengths of the thermally excited undulation modes. As noted above, this allows us to greatly simplify the hydrodynamics for the smectic-*A* phase.

The formulation of the linearized hydrodynamics for the smectic-*A* phase can be found, for instance, in Ref. [23]. Here we only recall the main assumptions needed in the derivation of the dynamic displacement-displacement correlation function in Fourier space. The new results concerning the

dynamic density-density correlation function in the thermodynamic limit are contained in Appendix A.

In the Fourier representation, we find [18,23] the following coupled equations for the local component of the velocity in the z direction v_z, and for the local displacement field u,

$$\frac{\partial u(\mathbf{q},t)}{\partial t} = v_z(\mathbf{q},t) \tag{10}$$

and

$$\rho_0 \frac{\partial v_z(\mathbf{q},t)}{\partial t} = -\eta_3 q_\perp^2 v_z(\mathbf{q},t) - (Bq_z^2 + Kq_\perp^4) u(\mathbf{q},t). \tag{11}$$

Here, ρ_0 is the average mass density, and η_3 is the layer sliding viscosity, which is the one viscosity that does not diverge in the low-frequency limit [18]. These equations make intuitive sense. The first one says that the layers move up at the same rate as the local fluid does, i.e., that permeation can be neglected. The second equation is just Newton's second law for the acceleration along the z direction in terms of the elastic and viscous forces that act along the z direction. The first term on the right-hand side of Eq. (11) is the viscous drag, and the second term is the elastic force, exerted on the smectic layers. Note that there is no equation for the density, since it has been assumed that it adjusts to the layer distortions. In fact, these equations can be simplified even further since the acceleration term on the left-hand side of Eq. (11) is much smaller than the force terms on the right-hand side. Neglecting the inertial term, we can easily obtain the velocity associated with the mode $\mathbf{q}$, which is given by

$$v_z(\mathbf{q},t) = -\frac{(Bq_z^2 + Kq_\perp^4)}{\eta_3 q_\perp^2} u(\mathbf{q},t). \tag{12}$$

To check the self-consistency of this assumption—i.e., to check whether the inertial term $\partial_t v_z$ is negligible—we can calculate it directly using Eq. (12). Then we find

$$\frac{\partial v_z(\mathbf{q},t)}{\partial t} = -\frac{(Bq_z^2 + Kq_\perp^4)}{\eta_3 q_\perp^2} v_z(\mathbf{q},t). \tag{13}$$

In the wave-vector regime we are interested in, $Bq_z^2 \sim Kq_\perp^4$. Therefore, using Eqs. (11) and (13) we find that $\rho_0 |\partial v_z/\partial t| \ll \eta_3 q_\perp^2 |v_z|$, provided that

$$\frac{\rho_0 K}{\eta_3^2} \ll 1. \tag{14}$$

This is clearly true for typical thermotropic parameters: $\rho_0 \approx 1\ \mathrm{g\ cm^{-3}}$, $K \approx 10^{-6}$ dyn, and $\eta_3 \approx 1\ \mathrm{g\ cm^{-1}\ s^{-1}}$, for which $\rho_0 K/\eta_3^2 \approx 10^{-6}$. Having established that we *are* in the extreme overdamped limit, we can use Eq. (12) in Eq. (10), which gives

$$\frac{\partial u(\mathbf{q},t)}{\partial t} = -\left(\frac{Bq_z^2 + Kq_\perp^4}{\eta_3 q_\perp^2}\right) u(\mathbf{q},t). \tag{15}$$

Now we multiply both sides of this equation by $u(\mathbf{q},0)$, and then take the thermal average to obtain

$$\langle u(\mathbf{q},t) u(-\mathbf{q},0)\rangle = \langle u(\mathbf{q},0) u(-\mathbf{q},0)\rangle \exp(-t/\tau_q), \tag{16}$$

where the relaxation time τ_q for the mode is given by [23]

$$\tau_q = \frac{\eta_3 q_\perp^2}{Bq_z^2 + Kq_\perp^4}. \tag{17}$$

Note that the relaxation time of the undulation mode diverges in the limit of small $q_\perp$. This is a direct consequence of the slow Goldstone mode associated with the broken translational symmetry. Also note that, for this equation, which applies in the thermodynamic limit, we have not needed to consider any boundary conditions. In the next section, we will consider the same linearized hydrodynamics for thin smectic-*A* films with surface tension and viscosity. As we noted in the Introduction, the finite-size boundary conditions, the surface tension, and the viscosity all play very important roles in the dynamic correlation functions for real films.

III. THE DYNAMIC CORRELATION FUNCTIONS FOR THE SMECTIC-*A* PHASE IN A FINITE-SIZE SYSTEM WITH SURFACE TENSION

A. The discrete model for finite-size smectic-*A* films

The freely suspended smectic-*A* liquid crystal films for which we are developing the finite-size theory in this section are perfectly quantized in the z direction (any partial layers are removed by the surface tension), but they have continuous two-dimensional fluid order in the two in-plane directions. Consequently, we will use the same one-dimensional discrete model for the z physics that we developed for our earlier work on the static correlation functions [5].

The Hamiltonian for the $(N+1)$-layer smectic-*A* discrete model [5] is given by

$$H = \tfrac{1}{2} \int d^2 r_\perp \Bigg\{ (B/d) \sum_{n=0}^{N-1} (u_{n+1} - u_n)^2 + dK \sum_{n=1}^{N-1} (\Delta_\perp u_n)^2 + \gamma[(\nabla_\perp u_0)^2 + (\nabla_\perp u_N)^2] + K_s[(\Delta_\perp u_0)^2 + (\Delta_\perp u_N)^2] \Bigg\}. \tag{18}$$

Here, u_n $(n = 0,\ldots,N)$ denotes the deviation of the nth layer from its equilibrium position, and the surface layer bend elastic constant K_s acts only at the two surface layers, i.e., at $n=0$ and $n=N$. Of course, in general, K_s can be different from Kd. The unperturbed layers are parallel to the xy plane, and we will consider u_n as a function of both the continuous variable $\mathbf{r}_\perp = (x,y)$ and of the time t. The total force acting on the nth layer at point $\mathbf{r}_\perp$ has two contributions: the viscous contribution $\eta_3 \Delta_\perp \partial u_n/\partial t$, and the elastic contribution $-d^{-1}\delta H/\delta u_n$. This results in the following set of equations of motion:

$$\rho_0 \frac{\partial^2 u_n}{\partial t^2} = \eta_3 \Delta_\perp \frac{\partial u_n}{\partial t} + B \frac{u_{n+1} - 2u_n + u_{n-1}}{d^2} - K \Delta_\perp^2 u_n$$

for $n = 1,...,N-1$,

$$d\rho_0 \frac{\partial^2 u_0}{\partial t^2} = d\eta_3 \Delta_\perp \frac{\partial u_0}{\partial t} + B \frac{u_1 - u_0}{d} - K_s \Delta_\perp^2 u_0 + \gamma \Delta_\perp u_0, \tag{19}$$

$$d\rho_0 \frac{\partial^2 u_N}{\partial t^2} = d\eta_3 \Delta_\perp \frac{\partial u_N}{\partial t} + B \frac{u_{N-1} - u_N}{d} - K_s \Delta_\perp^2 u_N + \gamma \Delta_\perp u_N .$$

In our analysis, we will neglect the acceleration term, and we will use the translational invariance of the system in the xy plane, i.e., we will use

$$u_n(\mathbf{r}_\perp, t) = S^{-1/2} \sum_{\mathbf{q}_\perp} u_n(\mathbf{q}_\perp, t) \exp(-i \mathbf{q}_\perp \cdot \mathbf{r}_\perp), \tag{20}$$

where S is the area of the smectic film. It is convenient to rewrite the equations of motion in terms of the dimensionless time: $t \mapsto t \eta_3 d / \sqrt{KB}$, and it is also convenient to introduce the two dimensionless vectors $\mathbf{Q} = \sqrt{\lambda d}\, \mathbf{q}_\perp$ and $\mathbf{R} = \mathbf{r}_\perp / \sqrt{\lambda d}$, where this $\lambda = \sqrt{K/B}$. Then the Hamiltonian can be expressed in terms of the discrete Fourier representation as

$$H = \frac{B}{2d} \sum_{\mathbf{Q}} u^\dagger(\mathbf{Q}) M(Q) u(\mathbf{Q}). \tag{21}$$

Here, $u(\mathbf{Q})$ is the $(N+1)\times 1$ matrix with components $u_n(\mathbf{Q})$ $(n = 0,...,N)$, $u^\dagger(\mathbf{Q})$ is the matrix adjoint to $u(\mathbf{Q})$, and $M(Q)$ is the $(N+1)\times(N+1)$ tridiagonal symmetric matrix defined by

$$M_{00} = M_{NN} = a = 1 + \overline{\gamma} Q^2 + \overline{K}_s Q^4,$$

$$M_{nn} = b = 2 + Q^4, \tag{22}$$

$$M_{nn-1} = M_{nn+1} = -1 \quad \text{for } n = 1,...,N-1.$$

Here we have also introduced the dimensionless surface tension $\overline{\gamma} = \gamma / \sqrt{KB}$, and the dimensionless surface layer bend elastic constant $K_s = K_s / Kd$.

The equations of motion can now be rewritten in the very compact matrix form

$$Q^2 \frac{\partial u(\mathbf{Q}, t)}{\partial t} = -M(Q) u(\mathbf{Q}, t). \tag{23}$$

The formal solution is given by

$$u(\mathbf{Q}, t) = \exp[-tM(Q)/Q^2] u(\mathbf{Q}, t = 0). \tag{24}$$

The next step is to find the $N+1$ eigenvalues $\lambda^{(k)}(Q)$ and the associated eigenvectors $v^{(k)}(Q)$, of the matrix $M(Q)$, and then to expand the formal solution in terms of the eigenvectors of $M(Q)$, to obtain

$$u(\mathbf{Q}, t) = \sum_{k=0}^{N} u^{(k)}(\mathbf{Q}, t) v^{(k)}(Q). \tag{25}$$

Note that the decay of the kth normal component is simply given by

$$u^{(k)}(\mathbf{Q}, t) = u^{(k)}(\mathbf{Q}, 0) \exp\left[- \frac{t}{\tau^{(k)}(Q)} \right], \tag{26}$$

and that the associated relaxation time is given by

$$\tau^{(k)}(Q) = Q^2 / \lambda^{(k)}(Q). \tag{27}$$

B. The displacement-displacement correlation function

Now that we have obtained the detailed dynamics of the layer displacement modes, we can calculate the associated layer displacement–layer displacement correlation function for finite-size smectic-A films.

In the Fourier representation, the displacement-displacement correlation function is defined as

$$C_{nm}(Q, t) = \langle u_n(\mathbf{Q}, t) u_m(-\mathbf{Q}, 0) \rangle. \tag{28}$$

Here the equilibrium average is over all possible displacements at $t = 0$. The probability of a given configuration is proportional to $\exp(-H/k_B T)$. In terms of the normal coordinates, the Hamiltonian is given by

$$H = \frac{B}{2d} \sum_{\mathbf{Q}} \sum_{k=0}^{N} \lambda^{(k)}(Q) |u^{(k)}(\mathbf{Q})|^2. \tag{29}$$

Consequently, the dynamic displacement-displacement correlation function is given by

$$C_{nm}(Q, t) = \frac{dk_B T}{B} \overline{C}_{nm}(Q, t)$$

$$= \frac{dk_B T}{B} \sum_{k=0}^{N} [\lambda^{(k)}(Q)]^{-1} \times \exp\left[- \frac{t}{\tau^{(k)}(Q)} \right] v_n^{(k)}(Q) v_m^{(k)}(Q), \tag{30}$$

where the eigenvectors $v^{(k)}(Q)$ are normalized to unity.

C. The density-density correlation function

To obtain the corresponding density-density correlation function from the displacement-displacement correlation function, we start with the center-of-mass density operator [5], which is given by

$$\hat{\rho}(\mathbf{r}, t) = \rho_s \sum_{n=0}^{N} \delta(z - nd - u_n(\mathbf{r}_\perp, t)), \tag{31}$$

where ρ_s is the density of molecules in the smectic layer. The corresponding density-density correlation function, with its wave-vector component parallel to the z axis equal to q_z, is defined to be

$$G(r_\perp, q_z, t) = \langle \hat{\rho}(\mathbf{r}_\perp, q_z, t) \hat{\rho}(0, -q_z, 0) \rangle$$

$$= \rho_s^2 \sum_{n,m=0}^{N} \exp[i(n-m) d q_z]$$

$$\times \exp[-\tfrac{1}{2} q_z^2 g_{nm}(r_\perp,t)], \tag{32}$$

where $g_{nm}(r_\perp,t)=\langle[u_n(\mathbf{r}_\perp,t)-u_m(0,0)]^2\rangle$. In terms of the dimensionless distance R, g_{nm} is given by

$$g_{nm}(R,t)=\frac{k_BT}{2\pi\sqrt{KB}}\int_{Q_{\min}}^{Q_{\max}} Q\,dQ[\overline{C}_{nn}(Q,0)+\overline{C}_{mm}(Q,0) - 2J_0(QR)\overline{C}_{nm}(Q,t)], \tag{33}$$

where $Q_{\min}$ and $Q_{\max}$ are the lower and upper cutoffs, respectively, and J_0 denotes the zeroth-order Bessel function.

As shown in Appendix B, the matrix $\overline{C}_{nm}(Q,t)$ diverges like Q^{-2} for small wave vectors. Consequently, for $t\neq 0$, the lower limit of integration in Eq. (33) cannot be extended to zero as is usually done to obtain the static correlation function. However, to proceed, we can split the total $\overline{C}_{nm}(Q,t)$ into two parts, namely an asymptotic part and a regular part, as follows:

$$\overline{C}_{nm}(Q,t)=\overline{C}^{\rm as}_{nm}(Q,t)+\overline{C}^{\rm reg}_{nm}(Q,t) = \frac{1}{2\overline{\gamma}Q^2}\exp[-t/\tau^{(0)}(0)]+\overline{C}^{\rm reg}_{nm}(Q,t). \tag{34}$$

Here the relaxation time $\tau^{(0)}(Q)$ corresponds to the lowest eigenvalue for the symmetric modes $\lambda^{(0)}(Q)$, and the regular part $\overline{C}^{\rm reg}_{nm}(Q,t)$ is finite at $Q=0$. Since $\lambda^{(0)}(Q)\approx 2\overline{\gamma}Q^2/(N+1)$ as $Q\to 0$, the corresponding relaxation time has a finite limit for $Q\to 0$, which is given by

$$\tau^{(0)}(0)=\frac{N+1}{2\overline{\gamma}}. \tag{35}$$

However, the remaining eigenvalues for both the symmetric and the antisymmetric modes have nonzero limits as $Q\to 0$, and consequently the corresponding relaxation times vanish at $Q=0$.

As shown in Appendix B, the asymptotic form for $\tau^{(0)}$ follows from the rigorous solution of the eigenvalue and eigenvector problem. However, it can also be obtained in a more straightforward manner directly from the equations of motion Eq. (19). To show this, take the sum from $n=0$ to N of both sides of this equation. Then, in the Fourier representation, we find

$$\rho_0\frac{\partial^2\overline{u}}{\partial t^2}=-\eta_3 q_\perp^2\frac{\partial\overline{u}}{\partial t}-\frac{\gamma q_\perp^2}{(N+1)d}(u_0+u_N). \tag{36}$$

Here, $\overline{u}=\Sigma_{n=0}^{n=N}u_n/(N+1)$ is the center of mass of the film, and we have included only the leading terms in $q_\perp$. In the limit as $q_\perp\to 0$, the slowest mode corresponds to a shift of the whole film without compression. In this case, $(u_0+u_N)/2=\overline{u}$. Now if we also neglect the acceleration term (i.e., take the overdamped limit) the asymptotic formula Eq. (35) follows. Note that in Eq. (36), the internal structure of the smectic film does not explicitly appear—in other words, this equation could also describe the motion of an ordinary liquid film. We also note that the inertial term is dominated by damping only if $q_\perp$ exceeds some limiting value. We will show below that this limiting value is of the same order as our experimental resolution. Thus, in the following discussion, we shall assume the overdamped limit.

Similarly, $g_{nm}(R,t)$ can also be split into asymptotic and regular parts. Performing the straightforward integration, we obtain

$$g^{\rm as}_{nm}(R,t)=\frac{k_BT}{2\pi\gamma}\left\{[1-\exp(-t/\tau^{(0)}(0))]\ln\frac{\Lambda}{a_0}+\exp(-t/\tau^{(0)}(0))\int_0^{Q_{\max}}[1-J_0(QR)]\frac{dQ}{Q}\right\}. \tag{37}$$

Here only the leading dependence on Λ has been included. The regular part is given by

$$g^{\rm reg}_{nm}(R,t)=\frac{k_BT}{2\pi\sqrt{KB}}\int_0^{Q_{\max}} Q\,dQ[\overline{C}^{\rm reg}_{nn}(Q,0)+\overline{C}^{\rm reg}_{mm}(Q,0)-2J_0(QR)\overline{C}^{\rm reg}_{nm}(Q,t)], \tag{38}$$

where we have extended the lower limit of integration to zero. The density-density correlation function can now be expressed as a product of the regular and asymptotic parts, which are given by

$$G^{\rm reg}(R,q_z,t)=\rho_s^2\sum_{n,m=0}^{N}\exp[i(n-m)dq_z]\exp[-\tfrac{1}{2}q_z^2 g^{\rm reg}_{nm}(R,t)] \tag{39}$$

and

$$G^{\rm as}(R,q_z,t)=\left(\frac{a_0}{\Lambda}\right)^{y(t)}\exp\left\{-x(t)\int_0^{Q_{\max}}[1-J_0(QR)]\frac{dQ}{Q}\right\}, \tag{40}$$

respectively. Here, $x(t)=(k_BTq_z^2/4\pi\gamma)\exp(-t/\tau^{(0)}(0))$, and $y(t)=x(0)-x(t)$. For $r_\perp>a_0$, Eq. (40) can be written in an alternative form as

$$G^{\rm as}(R,q_z,t)=\left(\frac{a_0}{\Lambda}\right)^{y(t)}\left(\frac{\overline{a}_0}{R}\right)^{x(t)}\exp\left\{-x(t)\left[\int_0^{2\pi}[1-J_0(s)]\frac{ds}{s}-\int_{2\pi}^{2\pi R/\overline{a}_0}J_0(s)\frac{ds}{s}\right]\right\}, \tag{41}$$

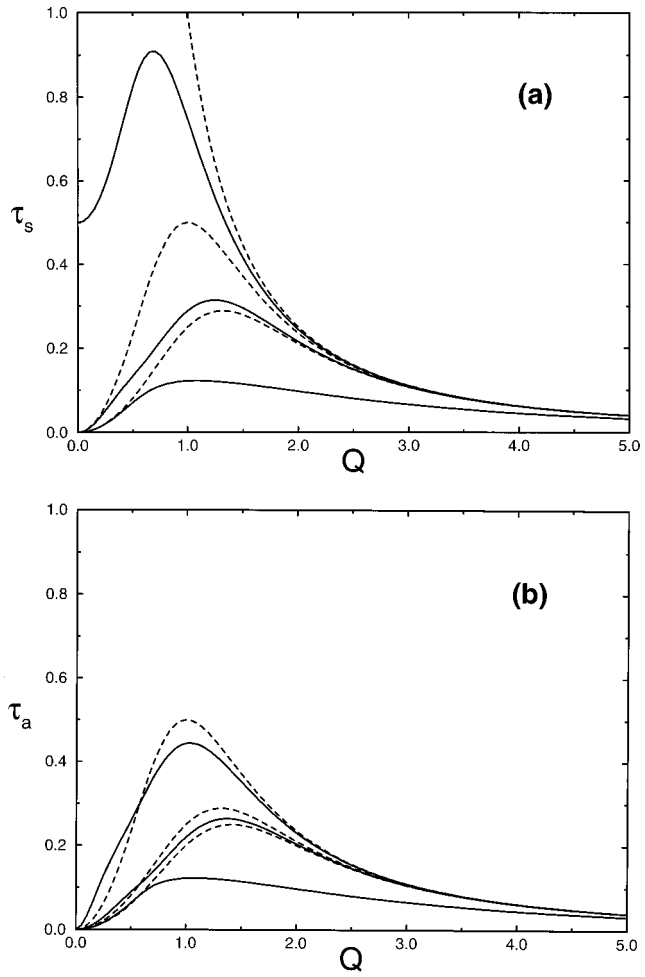

FIG. 1. The relaxation times of the symmetric (a) and the antisymmetric (b) modes versus Q for a smectic-A film with $N=5$. The solid and the dashed lines correspond to free and periodic boundary conditions, respectively. In all cases $\overline{\gamma}=6$ and $\overline{K}_s=1$ have been assumed.

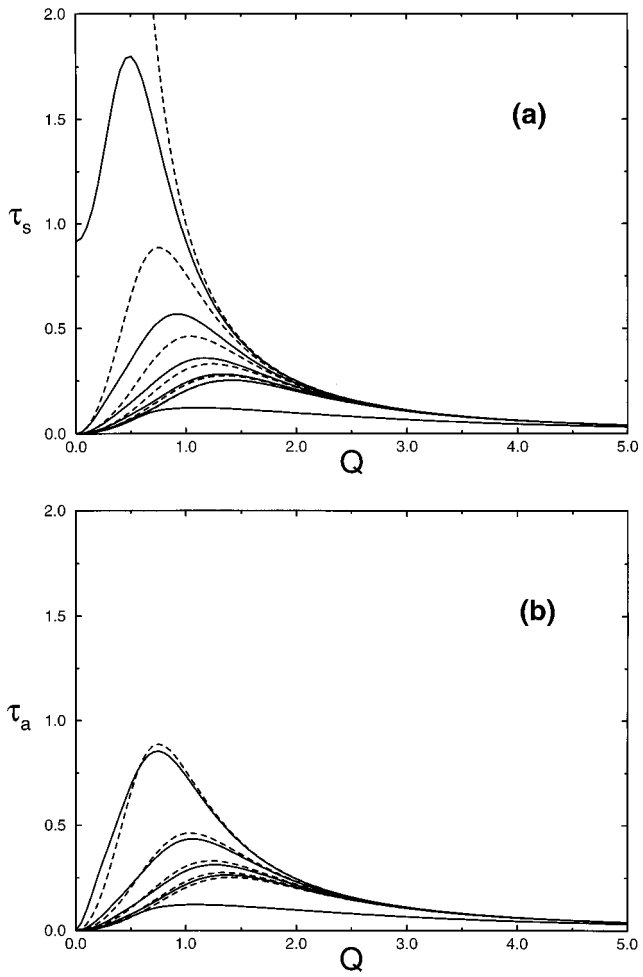

FIG. 2. The relaxation times of the symmetric (a) and the antisymmetric (b) modes versus Q for a smectic-A film with $N=10$. The solid and the dashed lines correspond to free and periodic boundary conditions, respectively. In all cases $\overline{\gamma}=6$ and $\overline{K}_s=1$ have been assumed.

from which the algebraic decay for $\overline{a}_0 \ll R \ll \overline{\Lambda}$ follows. Here, $\overline{a}_0 = a_0/\sqrt{\lambda d}$ and $\overline{\Lambda} = \Lambda/\sqrt{\lambda d}$.

The integral of the structure factor over $\mathbf{q}_\perp$ corresponds to $G(R=0,q_z,t)$, and thus we find that the scaling form of $G(R=0,q_z,t)$ is given by

$$G(R=0,q_z,t)=\left(\frac{a_0}{\Lambda}\right)^{y(t)} G^{\rm reg}(R=0,q_z,t). \qquad (42)$$

This means that the leading dependence on Λ is contained in the scaling factor, and that the evolution of this scaling factor is governed by $\tau^{(0)}(0)$.

In Figs. 1–3, we show the calculated relaxation times as functions of Q, for smectic films with $N=5$, 10, and 50 smectic layers. We display the relaxation times separately for the symmetric and the antisymmetric modes. For comparison, we also display the relaxation times calculated for periodic boundary conditions along the z axis, which are given by

$$\tau^{(k)}(Q)=\frac{Q^2}{2-2\cos[2\pi k/(N+1)]+Q^4}. \qquad (43)$$

Here, $k=0,...,N$, and all the times are shown in units of $\eta_3 d/\sqrt{KB}$, which are about 6×10^{-8} sec, for the typical thermotropic smectic-A parameters: $K=10^{-6}$ dyn, $B=2.5\times10^{7}$ dyn cm^{-2}, $\eta_3=1$ g cm^{-1} s^{-1}, and $d=30$ Å. For the case of free boundary conditions, and assuming that $\gamma=30$ dyn cm^{-1}, we find that $\tau^{(0)}(0)=(N+1)/12$. For $N=100$, this gives us the relaxation time $\tau_0\approx0.5\times10^{-6}$ sec.

In the case of the antisymmetric modes, the difference between films with free and periodic boundary conditions gradually disappears as N increases. Only the shortest relaxation time exhibits large deviations for $Q\geq1$. This is because, in the case of the free boundary conditions, eigenvectors of the form $v_n^{\pm}\propto z^n \pm z^{N-n}$ with z real appear if Q is sufficiently large, whereas $z=\exp(i\phi)$ for smaller values of Q (for details, see Appendix B).

The difference between the relaxation times of the symmetric modes, for free vs periodic boundary conditions, is much more dramatic. For periodic boundary conditions, the longest relaxation time exhibits a Q^{-2} divergence near $Q=0$, whereas, for free boundary conditions, the longest relaxation time remains finite at $Q=0$.

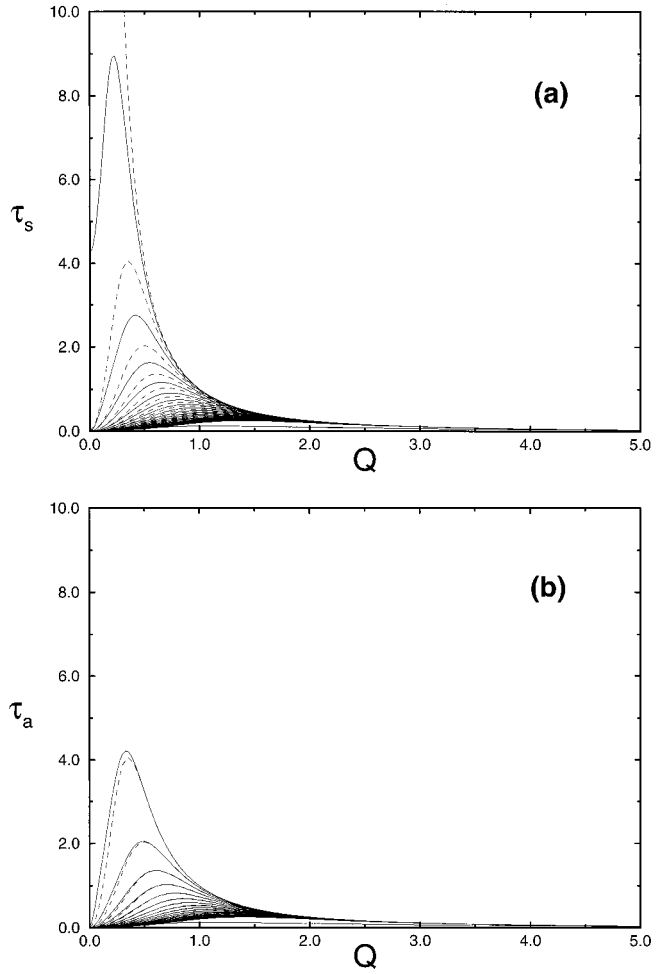

FIG. 3. The relaxation times of the symmetric (a) and the antisymmetric (b) modes versus Q for a smectic-A film with $N=50$. The solid and the dashed lines correspond to free and periodic boundary conditions, respectively. In all cases $\overline{\gamma}=6$ and $\overline{K_s}=1$ have been assumed.

IV. EXPERIMENTAL RESULTS

We have used soft-x-ray photon correlation spectroscopy to study the behavior of the thermally driven $q_\perp \to 0$ modes in the smectic-A phase of freely suspended liquid crystal films of two different materials: butoxybenzylidene octalaniline 4O.8 and heptyloxybenzylidene heptylaniline 7O.7. We measured the relaxation time of the fluctuations versus the film thickness for both 4O.8 and 7O.7.

The measurements were made using Beamline 7 at the Advanced Light Source Facility located at Lawrence Berkeley National Laboratory. The partially coherent soft-x-ray source on this beamline was a 5 cm period undulator operated to provide soft x rays with $\lambda = 44$ Å. The undulator was followed by a soft-x-ray monochromator that had an energy resolution of about 1 part in 10^4. This increased the longitudinal (temporal) coherence length from the value produced by the undulator, which was about 10^2 wavelengths or 4400 Å, to the value produced by the monochromator, which was about 10^4 wavelengths or 44 μm. The monochromatic beam was passed through a double pinhole filter to increase the transverse (spatial) coherence length. Essentially, the first pinhole makes position measurements of the photons, and the second pinhole makes transverse momentum measurements. Consequently, together these two pinholes defined the phase space occupied by the photons. The resulting coherence volume of our incident beam was about 40 by 40 by 44 μm, and the coherent intensity was typically $(5-10)\times 10^8$ photons per second.

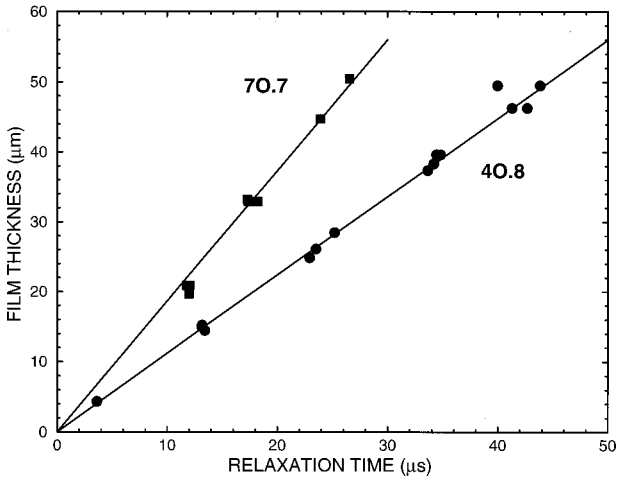

FIG. 4. Plot of the measured film thickness versus the measured relaxation times for freely suspended smectic-A films of 4O.8 (circles) and 7O.7 (squares). Our experimental data are in good agreement with our theoretical predictions presented in Sec. III.

The measurements were made by reflecting the coherent photons using the (001) Bragg reflections from the 4O.8 and 7O.7 films. The 2θ Bragg angles for both of these (001) reflections were about 100°. To detect the single soft-x-ray photons, we developed a special detector that coupled a fast scintillator to a photomultiplier. We used a two-channel logarithmic time-base digital autocorrelator to measure the intensity autocorrelation functions both for the Bragg reflected light and for the beam transmitted through the film. The transmitted beam intensity autocorrelation function was used to correct for the fluctuations in the beam from the synchrotron—we simply divided the Bragg scattering autocorrelation function by the transmitted beam autocorrelation function. Using this form of soft-x-ray photon correlation spectroscopy, we measured the fluctuations in the Bragg scattered light due to the thermally driven surface tension modes. For each film thickness, we fit the measured fluctuations to a simple exponential decay curve to determine the relaxation time. To determine the thickness of each film, we measured the soft-x-ray transmission through it, and then we used tabulated soft-x-ray-absorption coefficients to calculate the thickness of each film from our measured soft-x-ray absorption.

The results of our measurements are shown in Fig. 4, where we have plotted the measured film thicknesses in micrometers versus the measured relaxation times in microseconds. According to the theory developed in Sec. III, the relationship between the film thickness L and the relaxation time τ is given by

$$\tau = \left[\frac{\eta_3}{2\gamma}\right] L. \tag{44}$$

The straight line behavior shown in Fig. 4 clearly agrees with

this predicted linear dependence between L and τ. From the slopes of our measured data, we find

$$\left[\frac{2\gamma}{\eta_3}\right] = 112 \pm 11 \text{ cm/s} \quad \text{for } 4\text{O}.8 \tag{45}$$

and

$$\left[\frac{2\gamma}{\eta_3}\right] = 187 \pm 19 \text{ cm/s} \quad \text{for } 7\text{O}.7. \tag{46}$$

The surface tensions of 4O.8 and 7O.7 have both been measured [24], and they have the same measured surface tension (within the experimental errors), namely $\gamma = 21 \pm 0.2$ dyn/cm. Unfortunately, the layer sliding viscosities do not appear to have been measured for these two liquid crystals, so we cannot do the obvious direct quantitative test of our theory. However, we can still turn the problem around: by combining the measured value for the surface tension with the slopes of our measured thickness versus relaxation time plots, we find the following values for the layer sliding viscosities:

$$\eta_3 = 0.38 \pm 0.04 \text{ g/(cm s)} \quad \text{for } 4\text{O}.8 \tag{47}$$

and

$$\eta_3 = 0.23 \pm 0.02 \text{ g/(cm s)} \quad \text{for } 7\text{O}.7. \tag{48}$$

These values of the layer sliding viscosities for 4O.8 and 7O.7 are similar to previously measured values for the layer sliding viscosities of other smectic-A liquid crystals [25]. Since we do obtain straight lines with ''somewhat reasonable'' values for η_3, our experimental results support our theoretical predictions qualitatively—and ''somewhat'' quantitatively. Of course, direct independent measurements of η_3 for 4O.8 and 7O.7 will be even more convincing.

The overdamping assumed in this comparison merits some discussion. We argued in Sec. II that this overdamped limit is self-consistent in a bulk smectic. However, strictly speaking, in a finite smectic film, the inertial term in Eq. (19) cannot be neglected when $q_\perp$ becomes sufficiently small. In the presence of surface tension, we find that $\lambda^{(0)} \approx 2\gamma d q_\perp^2 / B(N+1)$, as $q_\perp \to 0$. So now, the new finite-size self-consistency condition can be written as

$$\frac{\rho_0 B \lambda^{(0)}}{d^2 \eta_3^2 q_\perp^4} \ll 1, \tag{49}$$

which breaks down as $q_\perp \to 0$. However, we can use Eq. (49) to determine the range of $q_\perp$ for which the inertial term is dominated by the viscous damping. This is given by $q_\perp \gg q_c$, where $q_c = [2\rho_0\gamma/\eta_3^2 d(N+1)]^{1/2} = [2/(N+1)]^{1/2} \times 10^4$ cm^{-1}. Note that we have used the asymptotic expression for $\lambda^{(0)}$, which is justified here since the surface tension term dominates the layer bend term as long as $q_\perp \ll [2\gamma/dK(N+1)]^{1/2} = [2/(N+1)]^{1/2} \times 10^7$ cm^{-1}. The length scale defined by q_c is comparable to the experimental resolution cutoff Λ.

In the near future, we plan to do experiments with much higher momentum transfer (i.e., ΔQ away from the Bragg peak), so that we can directly probe the thermally driven layer fluctuations. Note that the dynamics of these B and K modes cannot be probed in any other way. Unfortunately, this will greatly reduce the strength of our signal, so we will need to remove our monochromater and beamline; we estimate that this will give us at least a thousandfold increase in the input beam intensity, and thereby allow us to do the experiment.

V. DISCUSSION

In this paper, we have applied the linearized hydrodynamics of the smectic-A phase to determine the dynamic displacement-displacement and the dynamic density-density correlation functions both in the ideal thermodynamic limit and in the real world, finite-size, nonzero surface tension smectic-A film. To the best of our knowledge, this is the first time that these dynamic correlation functions have been presented in either case. We have also directly measured the thermally driven surface tension modes using coherent soft-x-ray photon correlation spectroscopy. The behavior that we have observed corresponds very nicely with our theoretical predictions. There are two clear items remaining on the experimental to-do list: (i) we should make independent measurements of η_3 to finalize the quantitative test of the overdamped limit of the theory, and (ii) we should extend our measurements so we can directly probe the thermally driven B and K modes.

We have also applied the linearized hydrodynamical description of the smectic-A phase to finite-size smectic-A films using a discrete version of the elastic Hamiltonian. We have shown that the longest relaxation time of these finite-size systems remains finite even in the infinite wavelength limit of the in-plane fluctuations. We show that the longest relaxation time remains finite both because of the finite size of the system in the normal direction, and also because of the presence of the surface tension. These results have important consequences, because the long-distance behavior of the density-density correlation function is governed by the long-wavelength behavior of the displacement-displacement correlation function. Originally, Caillé showed that the equal time density-density correlation functions decay algebraically with a nonuniversal exponent [1]. In contrast, we have shown that in the case of time-dependent correlation functions, the algebraic decay is governed by the time-dependent exponent $x(t)$. This behavior clearly differs from the predictions for the smectic-A phase in the thermodynamic limit, where the algebraic decay of the time-dependent density-density correlation function is governed by the same exponent as in the static case. This is because of the divergence of the relaxation time in the infinite wavelength limit.

We have also found an algebraic decay of the density-density correlation function with the resolution cutoff Λ. The exponent of that decay $y(t)$ goes to zero at $t=0$, and goes to $x(0) = k_B T q_z^2 / 4\pi\gamma$ in the limit as $t \to \infty$. For typical thermotropic parameters: $k_B T = 4 \times 10^{-14}$ erg, $\gamma = 30$ dyn cm^{-1}, $d = 30$ Å, and $q_z = 2\pi n/d$, we obtain $x(0) \approx 0.047 n^2$. Although this is a rather small number for $n=1$, it has a value around 0.2 for the second peak, which should be more accessible experimentally.

Finally, it will be interesting to study the Fourier transform of the density-density correlation function both in

space and time, and to study the higher-order correlation functions, which should be accessible in future experiments. However, because of the extraordinary amounts of computational work required to perform these studies, we must defer these problems to the future.

ACKNOWLEDGMENTS

We gratefully acknowledge the partial support of this work by KBN Grant Nos. 3T09A07212 and 2P03B01810, by the U.S. Department of Energy under Grant No. DE-FG06-86ER-45275, and by the NSF under Grant No. DMR-96-34596. We also gratefully acknowledge the U.S. Department of Energy's support of the Advanced Light Source Facility.

APPENDIX A

In this appendix, we derive the real-space, real-time two-point density autocorrelation function in a bulk smectic, and its spatio-temporal Fourier transform.

The electron density $\rho_e(\mathbf{r},t)$ in a smectic is given by

$$\rho_e(\mathbf{r},t)=\Psi(\mathbf{r},t)e^{iq_0z}+\rho_0+\text{c.c.}, \tag{A1}$$

where

$$\Psi(\mathbf{r},t)=|\Psi(\mathbf{r},t)|e^{iq_0u(\mathbf{r},t)}. \tag{A2}$$

Here, $u(\mathbf{r},t)$ is the local displacement field of the layers, $|\Psi(\mathbf{r},t)|$ is the local amplitude of the density wave, ρ_0 is the background density, and c.c. stands for complex conjugate. Now in the smectic phase itself—i.e., well below the nematic-to-smectic-*A* phase transition—the fluctuations in the amplitude $|\Psi(\mathbf{r},t)|$ are negligible. In fact, this is always a good approximation at sufficiently small q and ω—i.e., for $q\xi\ll 1$ and $\omega\tau\ll 1$, where $\xi(T)$ and $\tau(T)$ are the temperature-dependent correlation lengths and relaxation times, respectively. Of course, there are *two* correlation lengths, $\xi_\perp$ and ξ_z, in the nematic and the smectic-*A* phases, due to the anisotropic structure of these two phases.

We will restrict ourselves to this ''hydrodynamic limit'' where $q_\perp\xi_\perp$, $q_z\xi_z$, and $\omega\tau$ are all $\ll 1$, and we will ignore fluctuations in $|\Psi(\mathbf{r},t)|$. We then have

$$\begin{aligned}G_e(\mathbf{r},t)&=\langle\rho_e(\mathbf{r},t)\rho_e(\mathbf{0},0)\rangle\\&=|\Psi|^2\langle e^{iq_0[u(\mathbf{r},t)-u(\mathbf{0},0)]}\rangle e^{iq_0z}+\text{c.c.}\end{aligned} \tag{A3}$$

We proceed by approximating the fluctuations in u as Gaussian and accurately described by harmonic elastic theory and linearized hydrodynamics [26]. We will also use linearized hydrodynamics to treat the *dynamics* of the u field [27]. Given this, the fluctuations in $u(\mathbf{r},t)$ are Gaussian for all times—they are Gaussian at $t=0$ because the elasticity is harmonic, and they remain Gaussian at later times because the dynamics is linear. Hence we can use the general result that for any Gaussian variable x, $\langle\exp(x)\rangle=\exp(\langle x^2\rangle/2)$, provided that $\langle x\rangle=0$. Thus, we can simplify Eq. (A3) for $G_e(\mathbf{r},t)$ to

$$G_e(\mathbf{r},t)=|\Psi|^2\,\exp\{-\tfrac{1}{2}q_0^2\langle[u(\mathbf{r},t)-u(\mathbf{0},0)]^2\rangle\}, \tag{A4}$$

where we have also neglected the fluctuations in $\langle|\Psi(\mathbf{r},t)|^2\rangle$, for the reasons given earlier. Hence, our problem reduces to calculating

$$I(\mathbf{r},t)\equiv\langle[u(\mathbf{r},t)-u(\mathbf{0},0)]^2\rangle. \tag{A5}$$

By Fourier transforming *in space*,

$$u(\mathbf{r},t)\equiv\int\frac{d^3q}{(2\pi)^3}\,u(\mathbf{q},t)e^{i\mathbf{q}\cdot\mathbf{r}}, \tag{A6}$$

we can rewrite this as [see Eqs. (9) and (16) of Sec. II]

$$I(\mathbf{r},t)=2k_BT\int\frac{d^3q}{(2\pi)^3}\frac{1-\exp(-t/\tau_q)\cos(\mathbf{q}\cdot\mathbf{r})}{Bq_z^2+Kq_\perp^4}, \tag{A7}$$

where $\tau_q=\eta_3q_\perp^2/(Bq_z^2+Kq_\perp^4)$.

Evaluating the integrals over $\mathbf{q}$, we obtain

$$I(\mathbf{r},t)=\frac{k_BT}{4\pi\sqrt{BK}}\left[2\ln\left(\frac{r_\perp}{a_0}\right)-g\left(\frac{2\sqrt{BK}}{\eta_3}\frac{t}{|z|},\frac{r_\perp^2}{4\lambda|z|}\right)\right], \tag{A8}$$

with

$$g(x,y)\equiv\text{Ei}(-y)-\tfrac{1}{4}f(x,y), \tag{A9}$$

where

$$\text{Ei}(-y)\equiv-\int_y^\infty\frac{e^{-u}}{u}\,du \tag{A10}$$

is the ''exponential integral'' function [28], and where

$$f(x,y)\equiv\int_0^x\frac{du}{\sqrt{1+u^2}}\exp\left(-\frac{yu}{1+u^2}\right)I_0\left(\frac{yu}{1+u^2}\right). \tag{A11}$$

Here, $I_0(z)$ is the Bessel function of imaginary argument [28].

Using this result for $I(\mathbf{r},t)$ in Eq. (A4), we obtain

$$G_e(\mathbf{r},t)=|\Psi|^2\left(\frac{r_\perp}{a_0}\right)^{-2\eta}h\left(\frac{2\sqrt{BK}t}{\eta_3|z|},\frac{r_\perp^2}{4\lambda|z|}\right), \tag{A12}$$

where

$$h(x,y)=\exp(\eta g(x,y)) \tag{A13}$$

and $\eta=q_0^2k_BT/(8\pi\sqrt{BK})$. This intimidating expression fortunately simplifies in several limits.

(i) Limit one:

$$r_\perp \ll \sqrt{\lambda|z|},$$

$$G_e(r_\perp \ll \sqrt{\lambda|z|},z,t) = |\Psi|^2 e^{\eta c}\left[\frac{8Kt}{\eta_3 a_0^2}+\frac{4}{a_0^2}\left(\frac{Kz^2}{B}+\frac{4K^2t^2}{\eta_3^2}\right)^{1/2}\right]^{-\eta} = \begin{cases} |\Psi|^2 e^{\eta c}\left(\dfrac{16Kt}{\eta_3 a_0^2}\right)^{-\eta}, & t \gg \dfrac{\eta_3|z|}{\sqrt{BK}} \\ |\Psi|^2 e^{\eta c}\left(\dfrac{4\lambda|z|}{a_0^2}\right)^{-\eta}, & t \ll \dfrac{\eta_3|z|}{\sqrt{BK}} \end{cases} \tag{A14}$$

where $c \approx 0.577$ is Euler's constant. High-resolution x-ray measurements can typically probe length scales up to at least 3000 Å. Taking z to be of this order, η_3 to be of order 1 g(cm s)$^{-1}$, B to be 5×10^7 dyn cm^{-2}, and K to be 5×10^{-7} dyn, we obtain a crossover time $\eta_3|z|/\sqrt{BK} \sim 10^{-6}$ s, or, equivalently, a crossover frequency of about one megahertz. The values used in this estimate are typical values for *thermotropic* smectic liquid crystals; in lyotropic smectic liquid crystals, B can be 40 times larger.

(ii) Limit two:

$$r_\perp \gg \sqrt{\lambda|z|} \quad \text{and} \quad \sqrt{Kt/\eta_3},$$

$$G_e(r_\perp,z,t) = |\Psi|^2\left(\frac{r_\perp}{a_0}\right)^{-2\eta}. \tag{A15}$$

To summarize, the scaling forms of the dynamic density-density correlation function are given by

$$G_e(r_\perp,z,t) = \begin{cases} |\Psi|^2\left(\dfrac{4\lambda|z|}{a_0}\right)^{-\eta} e^{\eta c}, & |z|\to\infty \\ |\Psi|^2\left(\dfrac{16Kt}{\eta_3 a_0^2}\right)^{-\eta} e^{\eta c}, & t\to\infty \\ |\Psi|^2\left(\dfrac{r_\perp}{a_0}\right)^{-2\eta}, & r_\perp\to\infty. \end{cases} \tag{A16}$$

Note that the ratios of these various limits are known exactly once η is known.

In principle, inelastic x-ray scattering can be used to measure the spatio-temporal Fourier transform of $G_e(\mathbf{r},t)$. First, Fourier transforming in space gives

$$G_e(\mathbf{q},t) = \int d^3r\ e^{i\mathbf{q}\cdot\mathbf{r}} G_e(\mathbf{r},t). \tag{A17}$$

In general, this must be evaluated numerically. However, it can be shown to obey the scaling law

$$G_e(\mathbf{q},t) = q_\perp^{-4+2\eta}\Omega\left(\frac{2K|t|q_\perp^2}{\eta_3}, \frac{q_z-q_0}{\lambda q_\perp^2}\right), \tag{A18}$$

where the scaling function

$$\Omega(x,y) \equiv 2\frac{|\Psi|^2}{\lambda}\int_0^\infty dz \int_0^\infty dr_\perp r_\perp^{1-2\eta} \times h\left(\frac{x}{z}, \frac{r_\perp^2}{4z}\right)\cos(yz)J_0(r_\perp). \tag{A19}$$

Here J_0 is the zeroth-order Bessel function. $\Omega(x,y)$ must be evaluated numerically. To do so, we need to know the value of η, which can be obtained from the following two limits:

$$G_e(\mathbf{q},t) \propto q_\perp^{-4+2\eta}, \quad \frac{K|t|q_\perp^2}{\eta_3} \ll 1, \quad |q_z-q_0| \ll \lambda q_\perp^2 \tag{A20}$$

and

$$G_e(\mathbf{q},t) \propto |q_z-q_0|^{-2+\eta}, \quad \frac{\sqrt{BK}|t||q_z-q_0|}{\eta_3} \ll 1, \quad |q_z-q_0| \gg \lambda q_\perp^2. \tag{A21}$$

For example, fitting $G_e(\mathbf{q},t)$ to the power laws in these two limits will determine η. Then, the resulting η can be used to calculate the scaling function $\Omega(x,y)$ via Eq. (A19). Note that even without doing the full calculation, the scaling form given by Eq. (A18) can still be used to collapse an immense amount of data, and that the only fitting parameters are η, K/η_3 (which sets the time scale), and λ (which sets the length scale).

Fourier transforming in time as well gives

$$G_e(\mathbf{q},\omega) \equiv \int_{-\infty}^\infty dt\ e^{-i\omega t} G_e(\mathbf{q},t) = q_\perp^{-6+2\eta}\Phi\left(\frac{2Kq_\perp^2}{\eta_3\omega}, \frac{|q_z-q_0|}{\lambda q_\perp^2}\right), \tag{A22}$$

where

$$\Phi(x,y) \equiv \frac{|\Psi|^2\eta_3}{\sqrt{KB}}\int_0^\infty dt\ \cos(tx)\Omega(t,y). \tag{A23}$$

This also has simple scaling forms in a few limits,

$$G_e(\mathbf{q},\omega) \propto q_\perp^{-6+2\eta} \text{ when } \frac{Kq_\perp^2}{\eta_3\omega} \gg 1 \text{ and } \frac{|q_z-q_0|}{\lambda q_\perp^2} \ll 1, \tag{A24}$$

$$G_e(\mathbf{q},\omega) \propto q_z^{-3+\eta} \text{ when } \frac{\sqrt{KB}|q_z-q_0|}{\eta_3\omega} \gg 1 \text{ and } \frac{|q_z-q_0|}{\lambda q_\perp^2} \gg 1, \tag{A25}$$

$$G_e(\mathbf{q},\omega) \propto \omega^{-3+\eta} \text{ when } \frac{\sqrt{KB}|q_z-q_0|}{\eta_3\omega} \ll 1 \text{ and } \frac{Kq_\perp^2}{\eta_3\omega} \ll 1. \tag{A26}$$

For simplicity, Eqs. (A24), (A25), and (A26) are the $q_\perp \to \infty$, $|q_z - q_0| \to \infty$, and $\omega \to \infty$ limits, respectively.

APPENDIX B

In this appendix, we derive closed-form expressions for the eigenvalues and the eigenvectors of the coupled dynamical equations for finite-size smectic liquid crystals. To find the diagonal representation of $M(Q)$, we must solve the following set of equations:

$$\begin{aligned} -v_{n-1} + b v_n - v_{n+1} &= \lambda v_n \quad \text{for } n = 1,\ldots,N-1, \\ a v_0 - v_1 &= \lambda v_0, \\ -v_{N-1} + a v_N &= \lambda v_N . \end{aligned} \tag{B1}$$

Note that here, λ denotes an eigenvalue—which should not be confused with $\sqrt{K/B}$.

First, we verify that the eigenvectors are either symmetric or antisymmetric with respect to the transformation $n \mapsto N - n$. So, we must show that

$$v_n^{\pm} \propto z_k^n \pm z_k^{N-n}, \tag{B2}$$

where z_k is a root (real or complex) of one of the two polynomials

$$f_\pm(z) = z^{N+2} + \kappa z^{N+1} \pm (\kappa z + 1). \tag{B3}$$

Here, $\kappa = a - b = \bar{\gamma} Q^2 + (\bar{K}_s - 1) Q^4 - 1$. The eigenvalue corresponding to z_k is $\lambda^{(k)} = b - z_k - 1/z_k$. Since $\lambda^{(k)}$ must be real, z_k is either real or $z_k = \exp(i\phi_k)$. It can be shown that if $|\kappa| < 1$, then only the roots $z_k = \exp(i\phi_k)$ are possible. However, for $|\kappa| > 1$, some of the roots are real. From Eq. (B3), we see that $f_\pm(z) = \pm z^{N+2} f_\pm(1/z)$, hence all the roots appear in pairs of the form $(z_k, 1/z_k)$. In general, the roots of $f_\pm(z)$ can only be found numerically. However, it is possible to find a contour integral representation of $M(Q)$, which also leads to an explicit closed-form expression for $M^{-1}(Q)$.

To find the closed-form expression that we seek, we first introduce the projection matrices $P^\pm(z_k)$, which are given by

$$P^\pm_{nm}(z_k) = \mathcal{N}_\pm(z_k)(z_k^n \pm z_k^{N-n})(z_k^m \pm z_k^{N-m}). \tag{B4}$$

The normalization results from the condition $P^\pm(z_k)^2 = P^\pm(z_k)$, hence

$$\mathcal{N}_\pm(z_k) = \frac{1}{2}\left[\pm (N+1) z_k^N + \frac{z_k^{2(N+1)} - 1}{z_k^2 - 1} \right]^{-1}. \tag{B5}$$

Since $\mathcal{N}_\pm(1/z_k) = z_k^{2N} \mathcal{N}_\pm(z_k)$, we have $P^\pm(1/z_k) = P^\pm(z_k)$. Then using Eq. (B3), we find that

$$\mathcal{N}_\pm(z_k) = \pm \frac{z_k + \kappa}{2 f'_\pm(z_k)}. \tag{B6}$$

It is convenient to express $P^\pm(z_k)$ as

$$P^\pm_{nm}(z_k) = \frac{F^\pm_{nm}(z_k)}{f'_\pm(z_k)}, \tag{B7}$$

where

$$\begin{aligned} F^\pm_{nm}(z) = \pm \tfrac{1}{2}(z+\kappa)(z^{n+m} + z^{2N-n-m}) \\ + \frac{1}{2z^N}\left[(z+\kappa) z^{2N-|n-m|} + \frac{(\kappa z + 1)^2}{z^2(z+\kappa)} z^{|n-m|} \right]. \end{aligned} \tag{B8}$$

Here we have used the relation $z_k^{N+1} = \pm(\kappa z_k + 1)/(z_k + \kappa)$. Since all of the roots of the polynomials $f_\pm(z)$ are single roots (except for some special values of κ), we can treat the right-hand side of Eq. (B7) as a residue of the function $F^\pm_{nm}(z)/f_\pm(z)$ at $z = z_k$. Then we have

$$\frac{1}{2\pi i} \oint_C H_{nm}(z)\, dz = \sum_{k=0}^{N} [P_{nm}(z_k) + P_{nm}(1/z_k)] = 2\delta_{nm}, \tag{B9}$$

where

$$\begin{aligned} H_{nm}(z) = \frac{F^+_{nm}(z)}{f_+(z)} + \frac{F^-_{nm}(z)}{f_-(z)} = \frac{1}{f_+(z) f_-(z)} \{ -(z+\kappa)(\kappa z + 1)(z^{n+m} + z^{2N-n-m}) + (z+\kappa)^2 z^{2N-|n-m|+1} \\ + (\kappa z + 1)^2 z^{|n-m|-1} \}. \end{aligned} \tag{B10}$$

The contour of integration is chosen in such a way that all the roots of $f_\pm(z)$ are inside C, whereas outside C, $z = 0$. Depending on whether N is even or odd, either $z = 1$ or -1 are also roots of $f_\pm(z)$. However, it is easy to check that they are regular points of $H_{nm}(z)$. Thus, the sum in Eq. (B9) is over $2(N+1)$ roots of the polynomial $f_+(z) f_-(z)$, which are all distinct from $z = \pm 1$. That is to say, the sum is over $N+1$ pairs of the form $(z_k, 1/z_k)$, and P_{nm} corresponds to either P^+_{nm} or P^-_{nm}. Using this method, we can define a matrix function $\Phi(M)$ as follows:

$$[\Phi(M)]_{nm} = \frac{1}{2\pi i} \oint_C \Phi(\lambda(z)) \tfrac{1}{2} H_{nm}(z)\, dz, \tag{B11}$$

where $\lambda(z) = b - z - 1/z$, provided that $\Phi(\lambda(z))$ is holomorphic inside C. If we use the theorem that the sum of all the residues vanishes (including the residue at $z = \infty$), we can express $\Phi(M)$ as follows:

$$[\Phi(M)]_{nm} = -\tfrac{1}{2} \sum_{z \neq z_k} \mathrm{res}[\Phi(\lambda(z)) H_{nm}(z)], \tag{B12}$$

where the sum is over all singular points of the function $\Phi(\lambda(z))H_{nm}(z)$ other than the roots of $f_{\pm}(z)$.

Now we can easily find an explicit closed-form expression for the inverse matrix $M^{-1}(Q)$. We simply have

$$[M^{-1}]_{nm} = -\mathrm{res}[\lambda^{-1}(\zeta^{-1})H_{nm}(\zeta^{-1})] = \frac{\zeta^{-1}H_{nm}(\zeta^{-1})}{\zeta^{-1}-\zeta}, \tag{B13}$$

where $\lambda(\zeta)=\lambda(1/\zeta)=0$, $\zeta = 1+Q^4/2+Q^2\sqrt{1+Q^4/4}$. Because of the relation $H_{nm}(1/z) = -z^2 H_{nm}(z)$, the residues at $z=\zeta$ and $z=1/\zeta$ are equal. After some algebra, we find that

$$[M^{-1}]_{nm} = \frac{(1-\nu^2)(\zeta^{-n-m}+\zeta^{-2N+n+m}) + (1+\nu)^2\zeta^{-|n-m|} + (1-\nu)^2\zeta^{-2N+|n-m|}}{2Q^2\sqrt{1+Q^4/4}[(1+\nu)^2-(1-\nu)^2\zeta^{-2N}]}, \tag{B14}$$

where

$$\nu = \frac{\overline{\gamma} + (\overline{K}_s - 1/2)Q^2}{\sqrt{1+Q^4/4}}.$$

The above expression can be compared with the similar expression in Ref. [10] obtained for a continuous model of the smectic-*A* film. In that model, the authors used a continuous variable *z*, instead of a discrete layer index *n*, to describe the position of an unperturbed layer. In the limit of small *Q*—i.e., when $\zeta \approx \exp(Q^2)$ and $\nu \approx \overline{\gamma}$—both expressions have the same functional form. However, in the discrete model, the decay of $M^{-1}(Q)$ as $Q\to\infty$ is faster than in the continuum model. For example, in our discrete model, the diagonal components decay like Q^{-4}, whereas, in contrast, in the continuous model of Ref. [10] the diagonal components only decay like Q^{-2}, which leads to a logarithmic divergence of the displacement-displacement correlation function with the upper cutoff $Q_{\max}$. To avoid this divergence, an extra real-space cutoff was introduced in Ref. [10], which means that the *z* coordinate of a single layer is not defined precisely. In other words, in Ref. [10], it was assumed that the distance $|z-z'|$ between two layers has some minimal value, which was chosen to be $d/4$. However, in our discrete model, this problem does not appear, because the equilibrium position of every layer is well defined.

[1] A. Caillé, C. R. Seances Acad. Sci., Ser. B **274**, 891 (1972); also see the erratum in P. G. de Gennes, *The Physics of Liquid Crystals* (Oxford University Press, London, 1974), p. 336, Ref. 20.

[2] J. Als-Nielsen *et al.*, Phys. Rev. Lett. **26**, 1668 (1977); Phys. Rev. B **22**, 312 (1980); C. R. Safinya *et al.*, Phys. Rev. Lett. **57**, 2718 (1986).

[3] R. Hołyst, D. J. Tweet, and L. B. Sorensen, Phys. Rev. Lett. **65**, 2153 (1990).

[4] D. J. Tweet, R. Hołyst, B. D. Swanson, H. Stragier, and L. B. Sorensen, Phys. Rev. Lett. **65**, 2157 (1990).

[5] R. Hołyst, Phys. Rev. A **44**, 3692 (1991).

[6] J. M. Greif, D. L. Goodstein, and A. F. Silva-Moreira, Phys. Rev. B **25**, 6838 (1982).

[7] J. L. Cardy, Phys. Rev. B **26**, 6311 (1982).

[8] M. R. Fisch, P. S. Pershan, and L. B. Sorensen, Phys. Rev. A **29**, 2741 (1984).

[9] J. D. Shindler, E. A. Mol, A. Shalaginov, and W. H. de Jeu, Phys. Rev. Lett. **74**, 722 (1995).

[10] E. A. L. Mol, J. D. Shindler, A. N. Shalaginov, and W. H. de Jeu, Phys. Rev. E **54**, 536 (1996).

[11] A. Böttger, D. Frenkel, J. G. H. Joosten, and G. Krooshof, Phys. Rev. A **38**, 6316 (1988).

[12] A. N. Shalaginov and V. R. Romanov, Phys. Rev. E **48**, 1073 (1993).

[13] J.-C. Geminard, R. Hołyst, and P. Oswald, Phys. Rev. Lett. **78**, 1924 (1997).

[14] B. D. Swanson, H. Stragier, D. J. Tweet, and L. B. Sorensen, Phys. Rev. Lett. **62**, 909 (1989).

[15] B. D. Swanson and L. B. Sorensen, Phys. Rev. Lett. **75**, 3293 (1995).

[16] E. B. Sirota, P. S. Pershan, L. B. Sorensen, and J. Collett, Phys. Rev. Lett. **55**, 2039 (1985); Phys. Rev. A **36**, 2890 (1987).

[17] P. C. Martin, O. Parodi, and P. S. Pershan, Phys. Rev. A **6**, 2401 (1972).

[18] G. F. Mazenko, S. Ramaswamy, and J. Toner, Phys. Rev. Lett. **49**, 51 (1982); Phys. Rev. A **28**, 1618 (1983).

[19] G. Grinstein and R. Pelcovits, Phys. Rev. Lett. **47**, 856 (1981); Phys. Rev. A **26**, 915 (1982).

[20] K. Miyano, Phys. Rev. A **26**, 1820 (1982).

[21] P. Pierański *et al.*, Physica A **194**, 364 (1993).

[22] R. Hołyst, Phys. Rev. A **46**, 6748 (1992).

[23] P. G. de Gennes and J. Prost, *The Physics of Liquid Crystals*, 2nd ed. (Clarendon, Oxford, 1993), pp. 418 and 419.

[24] P. Mach *et al.*, J. Phys. II **5**, 217 (1995).

[25] P. Oswald, J. Phys. (France) **47**, 1091 (1986); C. Baumann, J. P. Marcerou, J. Prost, and C. Rouillon, Phys. Rev. Lett. **54**, 1268 (1985).

[26] This is, strictly speaking, not quite right: G. Grinstein and R. Pelcovits, Phys. Rev. A **26**, 915 (1982), showed that there are logarithmically diverging corrections to this approximation. However, the fractional changes are of order $(5w/64\pi)\ln(q_0/q)$, where *q* is the wavelength under consideration, and $w = k_B T B^{1/2}/K^{3/2}$. For the typical smectic values $B \sim 5\times10^7$ dyn/cm^2 and $K \sim 5\times10^{-7}$ dyn, one finds that at

room temperature $w \sim 0.8$. Hence, the fractional change due to this logarithmic divergence at $q = 10^{-3} q_0$ is only 14%. This corresponds to a length scale $2\pi/q$ of 10^3 $(2\pi/q_0) = 3$ μm. Of course, larger q's have even smaller corrections. So the harmonic approximation is a good one, except for unreasonably small q's, which are not probed in our experiment.

[27] This can be justified as well—as shown by G. Mazenko, S. Ramaswamy, and J. Toner, Phys. Rev. Lett. **49**, 51 (1982), and Phys. Rev. A **28**, 1618 (1983). Although there are *radical* changes to the dynamics due to nonlinearities in *most* wavevector and frequency regimes, those regimes that dominate the u fluctuations—which prove to be the regime $\omega \sim q_z \sim q_\perp^2$—are unaffected by the nonlinearities, except for the weak logarithmic Grinstein-Pelcovits effects on the statics alluded to earlier.

[28] I. S. Gradshteyn and I. M. Ryzhik, *Table of Integrals, Series, and Products* (Academic, New York, 1980), pp. 125 and 951.